Journal of Magnetic Resonance 197 (2009) 28–35

Contents lists available at ScienceDirect

Journal of Magnetic Resonance

journal homepage: www.elsevier.com/locate/jmr

Magnetic resonance in systems with equivalent spin-1/2 nuclides. Part 3: Ket analysis and spectral intensities

John A. Weil *, David F. Howarth

Department of Chemistry, University of Saskatchewan, 110 Science Place, Saskatoon, SK, Canada, S7N 5C9

ARTICLE INFO

Article history:
Received 18 April 2008
Revised 14 November 2008
Available online 3 December 2008

Keywords:
EPR
NMR
Hyperfine
Equivalent nuclides
Spin-hamiltonian energies and eigenstates
Exchange degeneracy
Spectral intensity

ABSTRACT

In earlier papers (Parts 1 and 2), featuring group-theoretical analysis, it was shown that the isotropic EPR spectra of free radical ($S = 1/2$) species XL_n, where the n equivalent nuclei also have spin 1/2, have a more complicated form than disclosed by the usual (first-order) oversimplified analysis. Explicit solutions for n = 3 (analytic, as well as computational) of the spin-hamiltonian matrix $\mathbf{H}_s$ for the energies and spin states were obtained and given in Part 2, but are amplified herein, and differences in several important representations of $\mathbf{H}_s$ are discussed. In the present work, we focus also on details of relative spectral intensities, some of which are not straightforward. Subtle asymmetry effects in relevant EPR spectra are demonstrated. The crucial factor here turns out to reside in the difference between field-swept and frequency-swept spectra, and hinges on the fact that $\mathbf{H}_s$ for the two states involved in any transition depends on Zeeman-field B as a variable in field-swept spectra, but B is a constant in frequency-swept spectra. An experimental spectrum of the free radical CF_3 is used as a quantitative example.

1. Introduction

This paper is a continuation of the earlier ones [1,2], in which we set out the problem, summarized the earlier literature, discussed various chemical examples (species XL_n in which the n ligand nuclei each have spin 1/2), and presented a group-theoretical as well as an analytical discussion. We believe that this project has considerable tutorial value. The problem is to quantify and understand the EPR spectra of free radical ($S = 1/2$) species XL_n, and also NMR spectra of analogous non-radical molecules, partly in clarification of common misunderstandings to be found in the literature. Nucleus X is taken to be spin-less. For paramagnetic XL_n with only one unpaired electron, there are $1 + n$ spins, $N = 2^{(1+n)}$ spin states, and $N(N-1)/2$ transition energies. Herein, one focus will be on certain details of the transition intensities. The spectral intensity of course is a second accessible observable, besides the quintessential line position information. In particular, the appreciable dependence on frequency of the relative peak intensities in EPR spectra (Fig. 1; also see Fig. 4 in Part 2 of this series) calls for analysis, to be discussed below. We wish to reiterate, as was stated in (1), that we only consider temperatures sufficiently high that no appreciable depopulation of low-lying rotational excited states is occurring, so that we may safely ignore quantum-statistical effects.

As discussed in Part 2 of the present series [NHW2008], the spin-hamiltonian operator for the XL_n system with one unpaired electron with spin $S = 1/2$ and n equivalent nuclei having spin $I = 1/2$ is given [[3], pp. 121,160; [4]] by

$$ {}^{\mathrm{op}}\mathrm{H}_s = {}^{\mathrm{op}}\mathrm{H}^{\mathrm{B}} + {}^{\mathrm{op}}\mathrm{H}^{\mathrm{hf}} + {}^{\mathrm{op}}\mathrm{H}^{n,\mathrm{ss}}(\mathrm{X},\mathrm{L}) \tag{1a} $$

$$ = \left(g\beta_e \mathbf{B}^{\mathrm{T}} \cdot {}^{\mathrm{op}}\mathbf{S} - g_n\beta_n \mathbf{B}^{\mathrm{T}} \cdot \sum_{i=1,n} {}^{\mathrm{op}}\mathbf{I}_i \right) + A\ {}^{\mathrm{op}}\mathbf{S}^{\mathrm{T}} \cdot \sum_i {}^{\mathrm{op}}\mathbf{I}_i + \sum_{i<j} J_{ij}\, {}^{\mathrm{op}}\mathbf{I}_i^{\mathrm{T}} \cdot {}^{\mathrm{op}}\mathbf{I}_j. \tag{1b} $$

The resulting energy levels are depicted in [NWH2005: Figs. 1 and 2], and for convenience can be labeled numerically 1, ..., 16 beginning at the top.

2. General aspects of EPR intensities

We wish in this work to pay particular attention to the theory underlying the relative intensities of the EPR lines stemming from the transitions between the spin states of a system XL_n, for arbitrary values of ligand number n. It should be noted that herein the system of n magnetically equivalent nuclei, all with spin 1/2, will be treated. This means that all nuclei within a set L have the same values of hyperfine coupling parameters A and effective nuclear g-factors g_n. Such equivalence can arise naturally from the symmetry of the molecule or through effective symmetry achieved by rapid internal motion.

* Corresponding author. Fax: +1 306 966 4730.
E-mail address: john.weil@usask.ca (J.A. Weil).

1090-7807/$ - see front matter © 2009 Published by Elsevier Inc.
doi:10.1016/j.jmr.2008.11.014

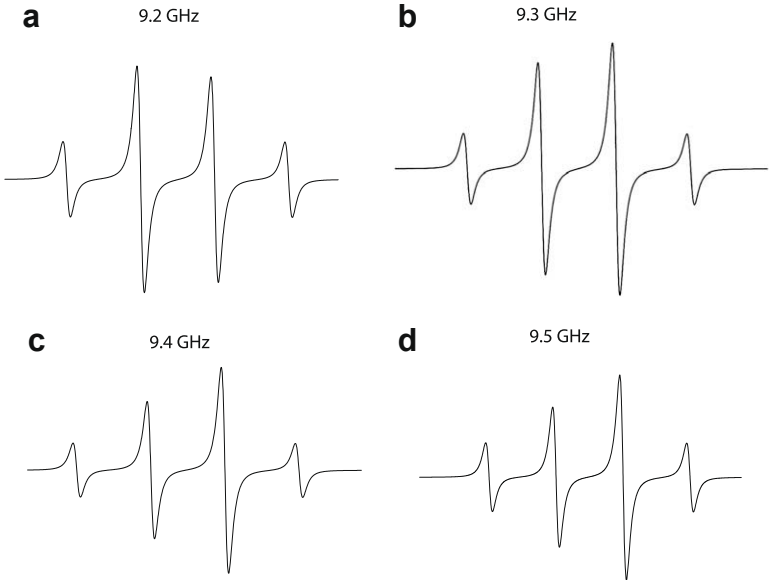

Fig. 1. The first-derivative field-swept EPR spectra, for a free-radical species XH_3, as produced by computer program EPR–NMR (7), for various X-band frequencies (in GHz): (a) 9.20, (b) 9.30, (c) 9.40, and (d) 9.50. The parameters $g = 2.0030$ and $A/(g_e\beta_e) = +0.500$ mT were utilized, with individual lines taken to be Lorentzians each with max–min width of 0.050 mT. The transitions at X-band, listed in order of increasing B field, are: 8–16, 5–15, {6,7–13,14}, 2–12, {3,4–10,11}, 1–9. The energy labels are defined as in [2], Appendix A.

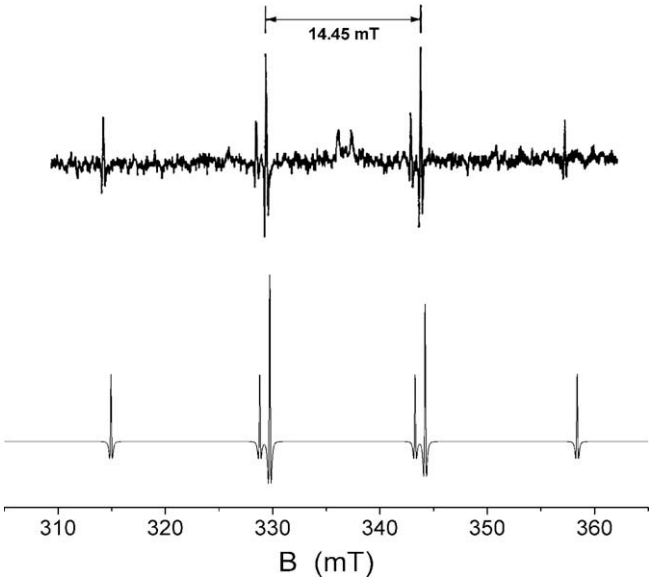

Fig. 2. The second-derivative field-swept EPR spectra for the free-radical species CF_3: (upper) photocopy of the experimental spectrum [8], and (lower) simulated Spectrum as produced by computer program EPR–NMR [7] with 8096 points, for frequency 9.452 GHz. The parameters $g = 2.00319$ and $A/(g_e\,\beta_e) = +14.481$ mT were taken from our best-fit of the Ref. [8] data, with individual lines taken to be Lorentzians each with max-min (first-deriv.) width of 0.15 mT. The value of $g_n(^{19}F)$ is positive. The 12 transitions, starting at lowest field ($B = 314.9365$ mT) are 1–16, 2–15, 3, 4 ⇔ 13, 4, 5–12, 6, 7 ⇔ 10, 11 and 8–9. The latter labels are taken in energy order appropriate for 315 mT, with 1 being the highest.

Once again placing special emphasis on n = 3, since it offers an excellent tractable example of the general case, keeping in mind the relevant energy-level scheme $E(B)$ (Fig. 1, in Part 1 of Ref. [1]) for XL_3, we note some special aspects of the underlying theory:

(a) There exist sets of energies which are degenerate, and which remain exactly superimposed for all applied magnetic-field values B and B_1.

(b) The B-independent degeneracy arises from the invariance of the spin-hamiltonian with respect to all sets of pairwise permutations of equivalent nuclei, i.e., it is the so-called 'exchange degeneracy' ([3], p. 391). It is absent for n = 1 and 2.

The 16×16 spin-hamiltonian matrix for XL_3 can be factored so that exact energy expressions are more easily available (Appendix A of Part 2).

Let us consider the transition energies and relative intensities of the EPR spectra of the XL_3 system. As was already mentioned in Part 2, the magnetic dipole transitions are allowed only between states which give non-zero matrix elements of the (electronic & nuclear) transition-moment operator ${}^{op}\mu_x = g\beta_e\ {}^{op}S_x - g_n\beta_n\Sigma_{i=1,n}{}^{op}I_{xi}$.

The magnetic excitation is taken herein with a linearly polarized magnetic field $\mathbf{B}_1$ (taken to be along $\mathbf{x}$) to be $\perp \mathbf{B} \parallel \mathbf{z}$. The details will not be discussed here [consult [4], and references found therein]. The non-zero matrix elements of ${}^{op}\mu_x$ occur only between states which belong to the same symmetry and for which $\Delta M_F = \pm 1$, (these two statements are the selection rules for the magnetic dipole transitions for such systems). For pure EPR, this becomes $\Delta M_S = \pm 1$.

The general theory of the transition probabilities of magnetic-dipole transitions can be found in the 'early' EPR literature, e.g. [5], as well as in more recent sources [6,4, chapters 4, 10]. Herein, we do not need or intend to deal with parameter anisotropies.

FORTRAN Program EPR–NMR [7] excels at best-fitting magnetic resonance line positions to produce spin-hamiltonian parameters. It is also capable of quantitatively evaluating the matrix elements of ${}^{op}\mu_x$, to deliver relative spectral intensities. We shall depend herein heavily on this capability. Use of EPR–NMR disclosed a very appreciable dependence for species XL_3 of the spectral intensities on the microwave excitation frequency, as may be seen for the middle lines of the 'quartets' depicted in Fig. 1, for EPR spectra at X-band (9–10 GHz). Tables 1 and 2 furnish details. The numerical normalization of the intensity data, as discussed in the manual for [7], is taken to be $[(g/g_e)|\langle a|S_x|b\rangle|]^2$, for transitions between states a and b.

Table 1
Computed line positions and intensities as functions of frequency for the field-swept EPR transitions of radical species XH_3, @ X-band, with $g = 2.0030$ and the $A/(g_e\beta_e)$ values = 0.50 mT. The transition label gives the two states involved, according to their energy. State #1 is highest in energy, and #16 is lowest. The uppermost twelve transitions are those for the major EPR lines, the next sixteen are pure NMR transitions, while the lowest five transitions correspond to those implied in Fig. 3 for the five 2×2 non-diagonal submatrices: EPR with simultaneous nuclear spin flips. All are of the σ type (15).

Transition label	Magnetic field B (mT)	Relative intensity (g, g_n on)	Total intensity of degenerate transitions
ν = 9.200 GHz			
8–16	327.4170	0.2502	
5–15	327.9161	0.2502	
6–13	327.9172	0.1854	0.5020
6–14		0.0633	
7–13		0.1988	
7–14		0.0545	
2–12	328.4159	0.2502	
3–10	328.4170	0.0313	0.4322
3–11		0.1284	
4–10		0.1180	
4–11		0.1545	
1–9	328.9165	0.2502	
2–16	326.9230	1.0220E−12	
1–15	327.4213	1.0221E−12	
9–12	215912.2358	1.7338E−6	
10–13	215912.2366	4.6402−7	2.0453E−6
10–14		4.5396E−7	
11–13		5.7393E−7	
11–14		4.5396E−7	
12–15	215912.2366	2.3117E−6	
15–16	215912.2369	1.7338E−6	
5–8	216241.3414	1.7285E−6	
2–5	216241.3421	2.3047E−6	
3–6	216241.3421	8.5921E−7	9.8092E−7
3–7		2.9541E−7	
4–6		1.1870E−8	
4–7		4.8089E−7	
1–2	216241.3425	1.7285E−6	
7–16	327.1700	1.4313E−40	
2–15	327.6681	1.1116E−27	
3–13	327.6693	1.0432E−27	3.1008E−27
4–14		2.0576E−27	
1–12	328.1676	2.9775E−35	
ν = 9.300 GHz			
8–16	330.9840	0.2502	
5–15	331.4831	0.2502	
6–13	331.4842	0.0907	0.5047
6–14		0.2061	
7–13		0.1487	
7–14		0.0592	
2–12	331.9829	0.2502	
3–10	331.9841	0.0526	0.6458
3–11		0.1105	
4–10		0.2444	
4–11		0.2383	
1–9	332.4835	0.2502	
2–16	330.4793	9.7879E−13	
1–15	330.9776	9.7881E−13	
9–12	218260.8966	1.7337E−6	
10–13	218260.8973	2.5575E−8	9.3445E−7
10–14		3.0053E−7	
11–13		2.8144E−7	
11–14		9.6725E−7	
12–15	218260.8973	2.3117E−6	
15–16	218260.8977	1.7337E−6	
5–8	218590.0022	1.7285E−6	
2–5	218590.0029	2.3047E−6	
3–6	218590.0029	5.3732E−7	1.9126E−6
3–7		4.5107E−7	
4–6		4.2174−7	
4–7		5.0251E−7	
1–2	218590.0033	1.7285E−6	
7–16	330.7316	7.9615E−38	
2–15	331.2298	3.7847E−28	
3–13	331.2309	2.7120E−27	3.8882E−27
4–14		1.1762E−27	
1–12	331.7292	6.1542E−37	
ν = 9.400 GHz			
8–16	334.5511	0.2502	
5–15	335.0502	0.2502	
6–13	335.0513	0.1119	0.3867
6–14		0.0585	
7–13		0.1802	
7–14		0.0361	
2–12	335.5500	0.2502	
3–10	335.5511	0.0579	0.7046
3–11		0.2202	
4–10		0.2228	
4–11		0.2036	
1–9		0.2502	
2–16	334.0355	9.3780E−13	
1–15	334.5338	9.3781E−13	
9–12	220609.5574	1.7337E−6	
10–13	220609.5581	3.9592E−7	9.5348E−7
10–14		4.7346E−7	
11–13		5.3607E−8	
11–14		3.0497E−8	
12–15	220609.5581	2.3116E−6	
15–16	220609.5585	1.7337E−6	
5–8	220938.6629	1.7286E−6	
2–5	220938.6636	2.3047E−6	
3–6	220938.6636	1.7185E−7	6.4660E−7
3–7		6.9554E−8	
4–6		2.9317E−7	
4–7		1.1203E−7	
1–2	220938.6640	1.7286E−6	
7–16	334.2933	1.4324E−39	
2–15	334.7914	1.6551E−28	
3–13	334.7925	7.2426E−29	3.8746E−27
4–14		3.8022E−27	
1–12	335.2909	3.7417E−34	
ν = 9.500 GHz			
8–16	338.1181	0.2502	
5–15	338.6172	0.2502	
6–13	338.6183	0.1202	0.2594
6–14		0.0618	
7–13		0.0010	
7–14		0.0764	
2–12	339.1170	0.2502	
3–10	339.1181	0.2459	0.4947
3–11		0.0977	
4–10		0.0608	
4–11		0.0903	
1–9	339.6176	0.2502	
2–16	337.5918	8.9893E−13	
1–15	338.0901	8.9895E−13	
9–12	222958.2181	1.7337E−6	
10–13	222958.2188	5.7319E−7	1.1765E−6
10–14		3.6170E−7	
11–13		1.9986E−7	
11–14		4.1750E−8	
12–15	222958.2188	2.3116E−6	
15–16	222958.2192	1.7337E−6	
5–8	223287.3237	1.7286E−6	
2–5	223287.3244	2.3048E−6	
3–6	223287.3244	4.6037E−7	1.8805E−6
3–7		5.7148E−7	
4–6		5.5583E−7	
4–7		2.9284E−7	
1–2	223287.3248	1.7286E−6	
7–16	337.8549	1.4988E−38	
2–15	338.3531	7.2266E−28	
3–13	338.3542	1.4243E−31	4.4632E−27
4–14		4.3208E−27	
1–12	338.8525	2.4665E−27	

Table 2
Computed line positions and intensities as functions of fixed magnetic field values B for the frequency-swept EPR transitions of XH_3 radical species, @ X-band, with $g = 2.0030$ and the $A/(g_e\beta_e)$ values = 0.50 mT. The transition label gives the two states involved, according to their energy. State #1 is highest in energy, and #16 the lowest. The uppermost twelve transitions are those for the major EPR lines, while the lowest five transitions correspond to those implied in Fig. 3 for the five 2×2 non-diagonal submatrices: EPR with simultaneous nuclear spin flips. All are of the σ type (15).

Transition label	Transition frequency (MHz)	Relative intensity (g, g_n on)	Total intensity of degenerate transitions
B = 328 mT			
8–16	9216.3445	0.2502	
5–15	9202.3534	0.2502	
6–13	9202.3214	0.0821	0.5002
6–14		0.1680	
7–13		0.1680	
7–14		0.0821	
2–12	9188.3409	0.2502	
3–10	9188.3089	0.0460	0.5004
3–11		0.2042	
4–10		0.2042	
4–11		0.0460	
1–9	9174.3071	0.2502	
7–16	9223.3037	3.7224E−38	
2–15	9209.3179	1.1156E−29	
3–13	9209.2859	1.7413E−26	1.7426E−26
4–14		1.3217E−29	
1–12	9195.2948	2.4048E−29	
B = 332 mT			
8–16	9328.4822	0.2502	
5–15	9314.4908	0.2502	
6–13	9314.4593	0.1801	0.5004
6–14		0.0701	
7–13		0.0701	
7–14		0.1801	
2–12	9300.4784	0.2502	
3–10	9300.4468	0.2155	0.5004
3–11		0.0347	
4–10		0.0347	
4–11		0.2155	
1–9	9286.4449	0.2502	
7–16	9335.6117	1.1944E−39	
2–15	9321.6256	6.7938E−28	
3–13	9321.5940	2.3903E−27	2.3908E−27
4–14		5.1226E−31	
1–12	9307.6026	1.5701E−35	
B = 336 mT			
8–16	9440.6200	0.2502	
5–15	9426.6283	0.2502	
6–13	9426.5971	0.0634	0.5004
6–14		0.1868	
7–13		0.1868	
7–14		0.0634	
2–12	9412.6159	0.2502	
3–10	9412.5846	0.0957	0.5004
3–11		0.1545	
4–10		0.1545	
4–11		0.0957	
1–9	9398.5826	0.2502	
7–16	9447.9198	8.6171E−40	
2–15	9433.9333	5.4003E−28	
3–13	9433.9021	6.7004E−28	7.5056E−28
4–14		8.0521E−29	
1–12	9419.9105	8.5396E−35	
B = 340 mT			
8–16	9552.7577	0.2502	
5–15	9538.7658	0.2502	
6–13	9538.7350	0.0780	0.5002
6–14		0.1721	
7–13		0.1721	
7–14		0.0780	
2–12	9524.7534	0.2502	
3–10	9524.7225	0.0080	0.5002
3–11		0.2421	
4–10		0.2421	
4–11		0.0080	
1–9	9510.7203	0.2502	
7–16	9560.2278	1.4287E−38	
2–15	9546.2411	4.9178E−30	
3–13	9546.2102	4.1405E−27	4.1438E−27
4–14		3.2772E−30	
1–12	9532.2184	3.9985E−29	

3. Analysis of CF_3 EPR

Experimental measurements allowing us to test our results on EPR intensities when degenerate spin states are present are very rare.

Happily, high-quality EPR spectra and analysis were presented by Fessenden and Schuler [8] in 1965 for free radical CF_3 ($S = 1/2$), created by irradiation. The solvent here is a liquid-phase perfluoroalkyl mixture. Their line-position (6 lines) data, in their Table 1, allows us to supercede their perturbation series analysis with the exact spin-hamiltonian matrix diagonalizations offered by program EPR–NMR. Using their line positions and microwave frequency, we found a nice agreement with the parameters obtained, theirs being $g = 2.0031$ and $A(^{19}F)/(g_e\beta_e) = 14.750$ mT, and ours being $g = 2.00319$ and $A/(g_e\beta_e) = +14.481$ mT. The rms deviation for the 6 lines at our best fit was 0.003 mT. The spacings between the inner-line sets of A and E state lines are 0.937 and 0.933 mT, respectively, consistent with the formula $3A^2/(2B)$ [see Fessenden [9]]. We note that Weltner ([10], pp. 142–143) also has discussed this spectrum.

We also point to comparing Fessenden & Schuler's experimental (slightly noisy) 2nd-derivative EPR spectrum with the simulated spectrum (Fig. 2) using the best-fit parameters produced by us via EPR–NMR. The agreement is excellent, including line positions *and* intensities. Note that the line asymmetries already alluded to are present, minor here but matching. As always, simulations of spectra are limited in accuracy by the need to use formal lineshape functions to simulate actual ones, and for CF_3 there lurks the specter of conceivably having six different line widths. The analogous free radical CH_3 has a considerably smaller ligand hyperfine parameter ($A/(g_e\beta_e) = -2.304$ mT). Its magnetic resonance features will be described elsewhere (and can be considered to be part #4 of the present series), due to its potential importance in radioastronomy.

4. Field scans versus frequency scans

In Table 1 we present the situation, obtained by use of program EPR–NMR, relevant when performing the field scans usually performed in EPR spectroscopy. We have tabulated four slightly different fixed frequency situations, all in the X-band region.

It is evident (Table 1) that the intensity changes sensitive to v occur for those transitions that take place between energy states belonging with the nuclear-spin state doublet irreducible representations E of permutation group P_3, and not those of the singlet type A. This then demands explanation.

In Table 2 we present the situation, described by use of program EPR–NMR, when using frequency scans, only rarely performed in EPR spectroscopy. We have tabulated four fixed field situations, all in the X-band region. We note some important differences between the contents of Tables 1 and 2. We see that now, in Table 2 but not in Table 1, there clearly are 'degeneracies' in the intensities amongst the four members of each degenerate-energy set. They occur in pairs. Also the total intensity in

each quartet of states here adds up to our 'magic' number $g/(2g_e)$: ca. 0.5000. The explanation of course is that for the fixed-field case, but not the fixed-frequency case, at each field there is a spin hamiltonian with only a single set of parameters. We note that the intensities of the two pairs of states that are intensity-degenerate do appear to misbehave, interchanging relative magnitudes as field B is changed: see Table 2. Only the total intensity of the set of four field-degenerate transitions is experimentally observable, so that this effect within the degenerate quartets cannot be observed.

5. Other results from program EPR–NMR, for species XL_3

We have also examined the theoretical EPR behavior at W-band, i.e., at 90–94 GHz, and find behavior of the inner lines varying with the frequency there much the same as we observed at X-band.

We investigated the effect of changing the sign of all three $A(^{19}F)$ values in the input from + to −, and found that this affected the intensities of the individual E-state transitions quite markedly, but left their line positions unaltered. However, the sum total of the four individual transitions of any given E set are much closer to being the same for both signs, so that sign measurement by this means would be difficult at X-band or higher frequencies.

Also for XL_3, removing the three nuclear Zeeman energy terms (but not the hyperfine couplings) did affect the EPR intensities with field sweep at X-band, but only very moderately, and did leave the line positions unaltered.

Presence in the transition moment operator of only the electron term $g\beta_e{}^{op}S_x$ suffices to yield the intensity asymmetry effects seen in field sweeps, i.e., the nuclear contributions to ${}^{op}\mu_x$ are not needed to do so.

We now proceed to examine especially the transitions between the pairs of doubly degenerate (E) states.

6. Presentation of the spin-hamiltonian

The spin-hamiltonian operator ${}^{op}H_s$ depends on the parameters A as well as on Zeeman energies $Y \equiv g\beta_e B/2$ and $Z \equiv g_n\,\beta_n B/2$, where for present purposes B is taken at some resonance line value. The latter of course is connected to the frequency ν of the "monochromatic" B_1 field deemed to be applied. Some characteristics of the spin-hamiltonian matrix $\mathbf{H}_s(A,Y,Z)$ can be found described in Appendix I. The types of eigenkets of $\mathbf{H}_s$ in various representations, and the inter-relations between these sets, is expounded in Appendix II.

The matrix $\mathbf{H}_s$ for XL_3 can be seen in explicit block-diagonal form in part 2 of this series [[2], Appendix A], as well as in diagrammatic form in the present work (Fig. 3). Here two of the four E-state 2×2 submatrices are already diagonal, and the other two such 2×2 matrices are not diagonal but are identical. Each of the latter has two distinct (non-identical) energy eigenvalues. We note that the eigenkets of the latter are not members of permutation-group basis of ${}^{op}H_s$, but rather are linear combinations thereof. None of the non-diagonal 2×2 matrices have eigenstates between which strongly allowed transitions take place (Tables 1 and 2). We also note that $\mathbf{H}_s$ becomes diagonal as $A/B \to 0$.

In summary, diagonalization of the 16×16 spin-hamiltonian matrix is routine. Of course, the diagonal form displays the four pairs of degenerate eigenvalues. We remember that no static magnetic field **B** will lift any of this degeneracy.

A crucial aspect of the frequency behavior resides in the diagonalization of ${}^{op}H_s$ when degenerate energy eigenvalues are involved. Here the admixture coefficients of the relevant spin kets are appreciably dependent on the resonant B values, i.e., on the frequency.

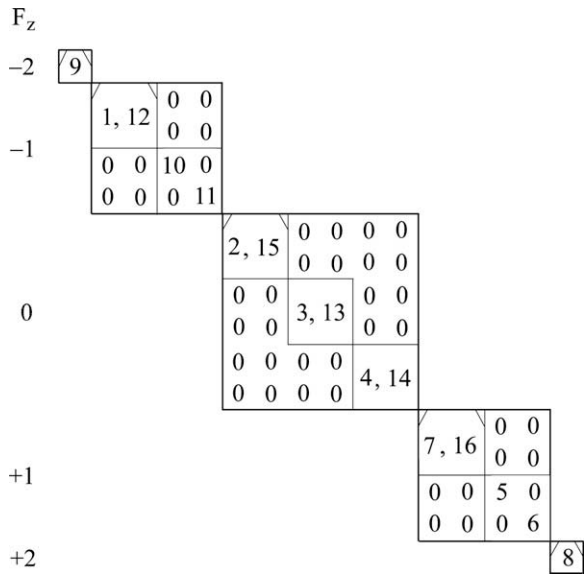

Fig. 3. Diagrammatic representation of the spin-hamiltonian matrix for XL_3 in a permutation-group basis (see Fig. 4). The submatrices involving states of type A are indicated with 'curtains'. The five 2×2 submatrices without any 0 are not diagonal, but show their eigenvalue labels. The four degenerate energy pairs are {10,11}, {3,4}, {13,14}, and {5,6}, which can be associated with quantum numbers $F_z = -1,0,0$ and +1, respectively. The energy labels are defined as in Ref. [2], Appendix A.

7. Frequency behavior of the magnetic resonance spectra intensities

To calculate transition intensities, it is necessary to evaluate the matrix elements of the transition moment operator ${}^{op}\mu_x$ brought in as a time-dependent (periodic) energy perturbation $-{}^{op}\mu_x B_1(t)$, *to be expressed* in the representation in which the spin-hamiltonian matrix is diagonal ([3], chapter 12; [11], chapter 3; [12], Section 2.3; [13], Appendix E). When there are energy-degenerate zeroth-order states, as in our case, the perturbation treatment requires some special manipulation. Success relies on avoiding situations yielding the 'blowing up' of any mathematical terms ([3], p. 231) that contain only the differences of the two equal energies, occurring in certain denominators. The degeneracy demands that the spin kets (or bras) for these states must be correctly combined ([14], chapter 3), for both the upper and the lower state involved in a given transition; this action is always possible. The admixture coefficients for handling each such 2×2 submatrix of any degenerate pair of states are functions of frequency ν. Hence the dependence of the final intensities on ν.

Happily, program EPR–NMR is equipped to handle degenerate spin states. Besides producing accurate line positions for fixed-frequency as well as fixed-field spectra, it produces the relative intensity of each. We note that the intensity of each line involving a degenerate set may differ from those of the others (Tables 1 and 2).

We see in Tables 1 that the splittings between the A and E transitions of both pairs of inner lines of each EPR spectrum remain constant and the same throughout the X-band region covered, whereas the intensities of the E lines (and not the A lines) vary dramatically and unequally for each pair. Hence the spectra become asymmetric. Finally, we note that in the present work (Tables 1 and 2, for XL_3), we have given much detail not only for the 12 primary EPR transitions ([2], Table 1), but also for the 16 other transitions, all of type $\Delta M_F = \pm 1$ (NMR), listed in Table 2 of [2]. These weak transitions arise because of the mixing of both the $M_S = \pm 1/2$ states into the same eigenket via the trig functions f

(see Appendix II), in 10 of the 16 kets φ. For good measure, we also include the 5 forbidden (see Appendix II, Section A) transitions between states arising from within the non-diagonal 2×2 boxes of the block-diagonal states of $\mathbf{H}_s$ (Fig. 3), which involve EPR accompanied by nuclear spin flips. We shall not discuss the intensities of the E-type lines found there, but expect that the arguments formulated herein do pertain to these also.

All the transitions cited in Tables 1 and 2 are of the σ type [15], transferring angular momentum between the spin systems and the photons involved.

8. Summary

Further details of the spin kets for molecule XL_3 have been tabulated and discussed. Also, we have seen and described subtle intensity changes with the frequency of the applied excitation field, which show up in field-swept EPR lines involving degenerate spin states. The spectral asymmetries do not show up in frequency-swept spectra. We have examined these line-intensity phenomena by means of computer-based quantitative techniques. We have succeeded in matching the subtle effects seen in an experimental spectrum.

We hope that the present work may stimulate much-needed further high-accuracy high-resolution EPR measurements of radicals such as CH_3 and CF_3, especially in liquid phase where g and A anisotropies are minimized. Then it will become easier to test and enhance our present theoretical notions.

Acknowledgments

We thank the Natural Sciences and Engineering Research Council (NSERC) of Canada for some support. The bulk of the project expenses were shouldered by one of the authors (JAW).

Appendix I. Representations of spin hamiltonians

Among the forms available to express the $N \times N$ spin-hamiltonian matrix $\mathbf{H}_s$, there are three especially useful ones.

A. Pure spin-basis form.
B. Permutation symmetry-adapted form
C. Diagonalized form

Transformation between these is accomplished via similarity transformations, using the respective eigenvectors. This is indicated diagrammatically in Fig. 4. In the above, positive integer N is the total number of spin states in the system.

In our case, for the isotropic molecular species XL_n, with static external applied field $\mathbf{B} \parallel \mathbf{z}$, the matrices $\mathbf{H}_s$ are all real and hence symmetric, and their N eigenvectors too are real.

A. The question arises as to how best to organize the matrix elements of $\mathbf{H}_s$ when there is a bevy of spins. One can select various ways of placing the pure spin kets in some logical order. One efficient way, used in program EPR–NMR [7], is described below.

The matrix elements are given row and column indices (the state numbers) via the following scheme. Let integer $\beta = 1,\ldots,$NSPINS label the spins (electrons and nuclei) and thus integer NSPINS indicates the total number of spins. Integer ${}^{\beta}\mathrm{d}$ is the number of states of spin β, i.e., ${}^{\beta}\mathrm{d} \equiv 2^{\beta}J + 1$. Thus $N = \Pi_{\beta=1,2,\ldots,\mathrm{NSPINS}}{}^{\beta}\mathrm{d}$. We shall utilize the individual spin-component quantum numbers ${}^{\alpha}m$, with the pre-superscript α used as a running index.

The indices $K = 1,2,\ldots,N$ of the rows and columns are correlated with the collections of spin-state quantum numbers according to auxiliary formula (valid for $N > 1$)

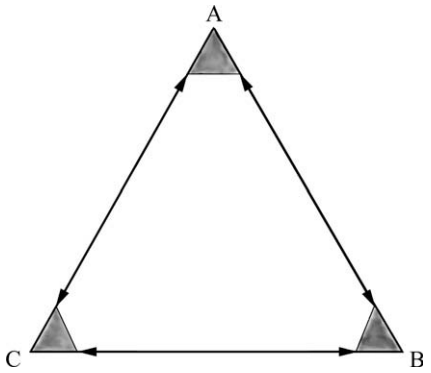

Fig. 4. A representation of three important representations of the spin-hamiltonian matrix $\mathbf{H}_s$ (see Appendix II). Apex A can denote a representation in which the basis for $\mathbf{H}_s$ is the set of the free spin kets as produced by program EPR–NMR [7], apex B the representation in which $\mathbf{H}_s$ is block diagonal according to the permutation symmetry, whereas C can represent the diagonalized representation of $\mathbf{H}_s$.

$$K' = ({}^{1}J + {}^{1}m)\prod_{\alpha=2}^{\mathrm{NSPINS}}{}^{\alpha}\mathrm{d} + ({}^{2}J + {}^{2}m)\prod_{\alpha=3}^{\mathrm{NSPINS}}{}^{\alpha}\mathrm{d} + \cdots + ({}^{\mathrm{NSPINS}-1}J + {}^{\mathrm{NSPINS}-1}m)^{\mathrm{NSPINS}}\mathrm{d}.$$

One thereby obtains a set of $N/2$ values of K', to each of which must be added +1 or +2 to obtain the complete set of K values.

Correspondingly, the scheme, used in program EPR–NMR, is:

Each index ${}^{\alpha}m$ will vary earlier with state number than indices ${}^{\alpha'}m$ having α' smaller than α, and later than indices ${}^{\alpha'}m$ having α' larger than α.

Thus, for matrix columns $1,\ldots,{}^{\beta=1}\mathrm{d}$, we first hold all ${}^{\alpha}m$ with $\alpha = 1,2,\ldots,$NSPINS -1 at their lowest values $-{}^{\alpha}J$ and vary ${}^{\mathrm{NSPINS}}m$ from $-{}^{\mathrm{NSPINS}}J$ by integers up to $+{}^{\mathrm{NSPINS}}J$.

For the next ${}^{\beta=2}\mathrm{d}$ columns, ${}^{\mathrm{NSPINS}}\mathrm{d} + 1,\ldots,2\,{}^{\mathrm{NSPINS}}\mathrm{d}$, indices ${}^{1}m$ through ${}^{\mathrm{NSPINS}-2}m$ are again held at $-{}^{\alpha}J$, ${}^{\mathrm{NSPINS}-1}m$ is held at $-{}^{\mathrm{NSPINS}-1}J + 1$, and ${}^{\mathrm{NSPINS}}m$ again varies as in the first ${}^{\mathrm{NSPINS}}\mathrm{d}$ columns, *etc.*

For a free-radical species XL_3 with four spins $J = 1/2$ (electron and 3 equivalent nuclei), the labeling of the columns and rows $1,\ldots,16$ occurs with spin states in the order (also see Appendix II):

$$|-,---\rangle, |-,--+\rangle, |-,-+-\rangle, |-,-++\rangle, |-,+--\rangle,$$
$$|-,+-+\rangle, |-,++-\rangle, |-,+++\rangle, |+,---\rangle, |+,--+\rangle,$$
$$|+,-+-\rangle, |+,-++\rangle, |+,+--\rangle, |+,+-+\rangle,$$
$$|+,++-\rangle, |+,+++\rangle .$$

These match with the eight values of $K' = 0,2,4,6,8,10,12$ and 14 when one adds separately +1 and +2 to each value.

B. In the block-diagonal matrix $\mathbf{H}_s$, the 5 submatrices in Fig. 3 herein appear in the order $F_z = +2,+1,0,-1,-2$. Here F_z is the z-component (quantum number M_F) of the total spin $\mathbf{F}$. This matrix is given in App. A of Part 2 (Ref. [2]) in the order $+2,-2,+1,-1,\ 0$.

C. Clearly, to diagonalize the matrix shown in Fig. 3, one needs only to diagonalize five 2×2 matrices, i.e., solve five quadratic equations, which can be done analytically and easily.

Appendix II. Inter-relations between sets of spin kets (See Fig. 4)

For a free-radical species XL_3 with four spins $J = 1/2$:

A. As stated on the previous page, the labeling of the columns and rows $1,\ldots,16$ of spin-hamiltonian matrix $\mathbf{H}_s$ (as prepared by Program EPR–NMR) occurs with spin states in the order

$|a_->\equiv|-,---\!>, |b_->\equiv|-,--+\!>, |c_->\equiv|-,-+-\!>,$
$|d_->\equiv|-,-++\!>, |e_->\equiv|-,+--\!>, |f_->\equiv|-,+-+\!>,$
$|g_->\equiv|-,++-\!>, |h_->\equiv|-,+++\!>, |a_+>\equiv|+,---\!>,$
$|b_+>\equiv|+,--+\!>, |c_+>\equiv|+,-+-\!>, |d_+>\equiv|+,-++\!>,$
$|e_+>\equiv|+,+--\!>, |f_+>\equiv|+,+-+\!>, |g_+>\equiv|+,++-\!>,$
$|h_+>\equiv|+,+++\!>.$

Most of these are not energy eigenkets except in the limit $A/B \to 0$.

We shall now 'complicate' the situation. As is true throughout our papers in the present series, we consider the case when the parameters A,g and g_n are all non-negative. It follows that, for B-field scans, there are two regions, defined by

Low field : $g_n\beta_n B < A$ and High field : $g_n\beta_n B > A$.

The 16 energy eigenstates of XL_3 are numbered to occur in the order of descending energy as: $\varphi_1 \ldots \varphi_8\ \varphi_9 \ldots \varphi_{16}$.

In the high-B region:

$$\varphi_1 = |+,---\!>\ldots\varphi_8 = |+,+++\!>\ \varphi_9 = |-,---\!>\ldots\varphi_{16} = |-,+++\!>.$$

Here the nuclear spins are quantized along the effective applied field $\mathbf{g}_n \cdot \mathbf{B}$.

However, in the low-B region, it would be physically more reasonable to quantize the nuclear spins along the direction $\mathbf{A}\cdot^{op}\mathbf{S}$. Then the kets would occur in order of descending energy as:

$$\varphi_1 = |+,+++\!>\ldots\varphi_8 = |+,---\!>\ \varphi_9 = |-,+++\!>\ldots\varphi_{16} = |-,---\!>.$$

The label crossing would occur at $B_L \equiv A/(g_n\beta_n)$ = 329.105 mT for protons when $A/(g_e\beta_e)$ = 0.5 mT (The typical value used herein). At that field, the 3 nuclear spin states cited in each ket would change projection signs. The four angles ξ (where ξ = any of $\delta_{1,2}$ and $\eta_{1,2}$: see Appendix II) in our example at $\mathbf{B}_L$ are all close to 0. The EPR frequency-swept spectrum at $\mathbf{B}_L$ consists of 6 distinct lines, with the primary spacings of $2Z/h \approx 14 \times 10^{-6}$ MHz. Note that the above labeling considerations remain implicit in both Tables 1 and 2.

Happily, in the isotropic case dealt with herein, we need not invoke matrices $\mathbf{g}_n$ and $\mathbf{A}$, and the field quantization axis can remain the same ($\mathbf{B}$) for all B values, and hence the above ideas remains academic.

B. The eigen-energies are listed in Appendix A of paper $XL_n - 2$ (Ref. [2]).

The energy-eigenkets for these, also given in [2], appear there and below in the block order:

$F_z = +2$
$\varphi_8 = |2,+2,{}^{+3/2}A_1\!> = |+,{}^{+3/2}A_1\!> = |+,+++\!>$
$F_z = -2$
$\varphi_9 = |2,-2,{}^{-3/2}A_1\!> = |-,{}^{-3/2}A_1\!> = |-,---\!>$
$F_z = +1$
$\varphi_5 = |2,+1,A_1^{i}\!> = \sin\delta_1|-,{}^{+3/2}A_1\!> + \cos\delta_1|+,{}^{+1/2}A_1\!>$
$\varphi_6 = |1,+1,{}^{+1/2}E_1\!> = |+,{}^{+1/2}E_1\!>$
$= (1/\sqrt{6})(2|+,-++\!> - |+,+-+\!> - |+,++-\!>)$
$\varphi_7 = |1,+1,{}^{+1/2}E_2\!> = |+,{}^{+1/2}E_2\!>$
$= (1/\sqrt{2})(|+,+-+\!> - |+,++-\!>)$
$\varphi_{16} = |1,+1,A_1^{ii}\!> = \cos\delta_1|-,{}^{+3/2}A_1\!> - \sin\delta_1|+,{}^{+1/2}A_1\!>$
$F_z = -1$
$\varphi_1 = |2,-1,A_1^{iii}\!> = \cos\delta_2|+,{}^{-3/2}A_1\!> + \sin\delta_2|-,{}^{-1/2}A_1\!>$
$\varphi_{10} = |1,-1,{}^{-1/2}E_1\!> = |-,{}^{-1/2}E_1\!>$
$= (1/\sqrt{6})(2|-,+--\!> - |-,-+-\!> - |-,--+\!>)$
$\varphi_{11} = |1,-1,{}^{-1/2}E_2\!> = |-,{}^{-1/2}E_2\!>$
$= (1/\sqrt{2})(|-,-+-\!> - |-,--+\!>)$
$\varphi_{12} = |1,-1,A_1^{iv}\!> = \cos\delta_2|-,{}^{-1/2}A_1\!> - \sin\delta_2|+,{}^{-3/2}A_1\!>$
$F_z = 0$
$\varphi_2 = |2,0,A_1^{v}\!> = \cos\eta_1|+,{}^{-1/2}A_1\!> + \sin\eta_1|-,{}^{+1/2}A_1\!>$
$\varphi_3 = |1,0,E_1^{i}\!> = \cos\eta_2|+,{}^{-1/2}E_1\!> - \sin\eta_2|-,{}^{+1/2}E_1\!>$
$\varphi_4 = |1,0,E_2^{i}\!> = \cos\eta_2|+,{}^{-1/2}E_2\!> - \sin\eta_2|-,{}^{+1/2}E_2\!>$
$\varphi_{13} = |0,0,E_1^{ii}\!> = \sin\eta_2|+,{}^{-1/2}E_1\!> + \cos\eta_2|-,{}^{+1/2}E_1\!>$
$\varphi_{14} = |0,0,E_2^{ii}\!> = \sin\eta_2|+,{}^{-1/2}E_2\!> + \cos\eta_2|-,{}^{+1/2}E_2\!>$
$\varphi_{15} = |1,0,A_1^{vi}\!> = \cos\eta_1|-,{}^{+1/2}A_1\!> - \sin\eta_1|+,{}^{-1/2}A_1\!>.$

In the above, the angles have been defined in Ref. [2], and the kets at the right side are:

$|\pm,{}^{+3/2}A_1\!> = |\pm,+++\!>$
$|\pm,{}^{+1/2}A_1\!> = (1/\sqrt{3})(|\pm,++-\!> + |\pm,+-+\!> + |\pm,-++\!>)$
$|\pm,{}^{-1/2}A_1\!> = (1/\sqrt{3})(|\pm,+--\!> + |\pm,-+-\!> + |\pm,--+\!>)$
$|\pm,{}^{-3/2}A_1\!> = |\pm,---\!>$
$|\pm,{}^{+1/2}E_1\!> = \pm(1/\sqrt{6})(2|\pm,-++\!> - |\pm,+-+\!> - |\pm,++-\!>)$
$|\pm,{}^{-1/2}E_1\!> = (1/\sqrt{6})(2|\pm,+--\!> - |\pm,-+-\!> - |\pm,--+\!>)$
$|\pm,{}^{+1/2}E_2\!> = \pm(1/\sqrt{2})(|\pm,+-+\!> - |\pm,++-\!>)$
$|\pm,{}^{-1/2}E_2\!> = (1/\sqrt{2})(|\pm,-+-\!> - |\pm,--+\!>).$

The eigenstate kets, sorted according to energy E, with E ranging from highest (#1) to lowest (#16) and taking g, g_n, $A > 0$, with B approaching $+\infty$, are: $\varphi_1, \varphi_2, \ldots, \varphi_{15}, \varphi_{16}$.

Hence, in terms of the free-spin kets, in the high-field region, the eigenkets in block order are:

$F_z = +2$
$\varphi_8 = |h_+\!>$
$F_z = -2$
$\varphi_9 = |a_-\!>$
$F_z = +1$
$\varphi_5 = \sin\delta_1|h_-\!> + \cos\delta_1(1/\sqrt{3})(|g_+\!> + |f_+\!> + |d_+\!>)$
$\varphi_6 = (1/\sqrt{6})(2|d_+\!> - |f_+\!> - |g_+\!>)$
$\varphi_7 = (1/\sqrt{2})(|e_+\!> - |g_+\!>)$
$\varphi_{16} = \cos\delta_1|h_-\!> - \sin\delta_1(1/\sqrt{3})(|g_+\!> + |f_+\!> + |d_+\!>)$
$F_z = -1$
$\varphi_1 = \cos\delta_2|a_+\!> + \sin\delta_2(1/\sqrt{3})(|e_-\!> + |c_-\!> + |b_-\!>)$
$\varphi_{10} = (1/\sqrt{6})(2|e_-\!> - |c_-\!> - |b_-\!>)$
$\varphi_{11} = (1/\sqrt{2})(|c_-\!> - |b_-\!>)$
$\varphi_{12} = \cos\delta_2(1/\sqrt{3})(|e_-\!> + |c_-\!> + |b_-\!>) - \sin\delta_2|a_+\!>$
$F_z = 0$
$\varphi_2 = \cos\eta_1(1/\sqrt{3})(|e_+\!> + |c_+\!> + |b_+\!>)$
$+ \sin\eta_1(1/\sqrt{3})(|g_-\!> + |f_-\!> + |d_-\!>)$
$\varphi_3 = \cos\eta_2(1/\sqrt{6})(2|e_+\!> - |f_+\!> - |b_+\!>)$
$+ \sin\eta_2(1/\sqrt{6})(2|d_-\!> - |f_-\!> - |g_-\!>)$
$\varphi_4 = \cos\eta_2(1/\sqrt{2})(|c_+\!> - |b_+\!>) + \sin\eta_2(1/\sqrt{2})(|f_-\!> - |g_-\!>)$
$\varphi_{13} = \sin\eta_2(1/\sqrt{6})(2|e_+\!> - |c_+\!> - |b_+\!>)$
$- \cos\eta_2(1/\sqrt{6})(2|d_-\!> - |f_-\!> - |g_-\!>)$
$\varphi_{14} = \sin\eta_2(1/\sqrt{2})(|c_+\!> - |b_+\!>) - \cos\eta_2(1/\sqrt{2})(|f_-\!> - |g_-\!>)$
$\varphi_{15} = \cos\eta_1(1/\sqrt{3})(|g_-\!> + |f_-\!>$
$+ |d_-\!>) - \sin\eta_1(1/\sqrt{3})(|e_+\!> + |c_+\!> + |b_+\!>).$

In terms of decreasing energy eigenvalues, one can then write the eigenkets in the high-field region as:

$$\varphi_1 = \cos\delta_2|a_+> + \sin\delta_2(1/\sqrt{3})(|e_-> + |c_-> + |b_->)$$
$$\varphi_2 = \cos\eta_1(1/\sqrt{3})(|e_+> + |c_+> + |b_+>) + \sin\eta_1(1/\sqrt{3})(|g_-> + |f_-> + |d_->)$$
$$\varphi_3 = \cos\eta_2(1/\sqrt{6})(2|e_+> - |c_+> - |b_+>) + \sin\eta_2(1/\sqrt{6})(2|d_-> - |f_-> - |g_->)$$
$$\varphi_4 = \cos\eta_2(1/\sqrt{2})(|c_+> - |b_+>) + \sin\eta_2(1/\sqrt{2})(|f_-> - |g_->)$$
$$\varphi_5 = \cos\delta_1(1/\sqrt{3})(|g_+> + |f_+> + |d_+>) + \sin\delta_1|h_->$$
$$\varphi_6 = (1/\sqrt{6})(2|d_+> - |f_+> - |g_+>)$$
$$\varphi_7 = (1/\sqrt{2})(|e_+> - |g_+>)$$
$$\varphi_8 = |h_+>$$
$$\varphi_9 = |a_->$$
$$\varphi_{10} = (1/\sqrt{6})(2|e_-> - |c_-> - |b_->)$$
$$\varphi_{11} = (1/\sqrt{2})(|c_-> - |b_->)$$
$$\varphi_{12} = \cos\delta_2(1/\sqrt{3})(|e_-> + |c_-> + |b_->) - \sin\delta_2|a_+>$$
$$\varphi_{13} = -\cos\eta_2(1/\sqrt{6})(2|d_-> - |f_-> - |g_->) + \sin\eta_2(1/\sqrt{6})(2|e_+> - |c_+> - |b_+>)$$
$$\varphi_{14} = \cos\eta_2(1/\sqrt{2})(|g_-> - |f_->) + \sin\eta_2(1/\sqrt{2})(|c_+> - |b_+>)$$
$$\varphi_{15} = \cos\eta_1(1/\sqrt{3})(|g_-> + |f_-> + |d_->) - \sin\eta_1(1/\sqrt{3})(|e_+> + |c_+> + |b_+>).$$
$$\varphi_{16} = \cos\delta_1|h_-> - \sin\delta_1(1/\sqrt{3})(|g_+> + |f_+> + |d_+>).$$

Since $\cos\xi = 1$ (where ξ = any of $\delta_{1,2}$ and $\eta_{1,2}$) in the limit as $B \to \infty$, we can easily attain from the above the ordered set of eigenkets in that limit, valid when g and g_n are non-negative.

From the above results, we can also solve for the free-spin expressions valid in the high-field region:

$$|a_-> = \varphi_9$$
$$|b_-> = (1/\sqrt{3})f_8 - (1/\sqrt{2})\varphi_8 - (1/\sqrt{2})\varphi_{11}$$
$$|c_-> = (1/\sqrt{3})f_8 - (1/\sqrt{2})\varphi_8 + (1/\sqrt{2})\varphi_{11}$$
$$|d_-> = (1/\sqrt{3})f_3 + (\sqrt{2}/\sqrt{3})\varphi_6 - \sqrt{3}f_{12} + (\sqrt{3}/\sqrt{2})f_{14}$$
$$|e_-> = (1/\sqrt{3})f_8 + \sqrt{2}\varphi_8$$
$$|f_-> = -1/(2\sqrt{3})f_3 + (1/\sqrt{6})\varphi_6 + (\sqrt{3}/2)f_{12} + (1/\sqrt{2})f_{16}$$
$$|g_-> = -1/(2\sqrt{3})f_3 + (1/\sqrt{6})\varphi_6 + (\sqrt{3}/2)f_{12} - (1/\sqrt{2})f_{16}$$
$$|h_-> = f_4$$
$$|a_+> = f_7$$
$$|b_+> = (1/\sqrt{3})f_{11} - (1/\sqrt{6})f_{13} - (1/\sqrt{2})f_{15}$$
$$|c_+> = (1/\sqrt{3})f_{11} - (1/\sqrt{6})f_{13} + (1/\sqrt{2})f_{15}$$
$$|d_+> = (1/\sqrt{3})f_3 + (\sqrt{2}/\sqrt{3})\varphi_6$$
$$|e_+> = (1/\sqrt{3})f_{11} + (\sqrt{2}/\sqrt{3})f_{13}$$
$$|f_+> = (2/\sqrt{3})f_3 - (\sqrt{2}/\sqrt{3})\varphi_6 - (1/\sqrt{3})f_{11} - (\sqrt{2}/\sqrt{3})f_{13} + \sqrt{2}\varphi_7$$
$$|g_+> = (1/\sqrt{3})f_{11} + (\sqrt{2}/\sqrt{3})f_{13} - \sqrt{2}\varphi_7$$
$$|h_+> = \varphi_8.$$

Here the ten auxiliary trig-function kets f are defined

$$f_3 \equiv \cos\eta_1\varphi_5 - \sin\eta_1\varphi_{16}$$
$$f_4 \equiv \cos\eta_1\varphi_{16} + \sin\eta_1\varphi_5$$
$$f_7 \equiv \cos\delta_2\varphi_1 - \sin\delta_2\varphi_{12}$$
$$f_8 \equiv \cos\delta_2\varphi_{11} + \sin\delta_2\varphi_1$$
$$f_{11} \equiv \cos\delta_1\varphi_2 - \sin\delta_1\varphi_{15}$$
$$f_{12} \equiv \cos\delta_1\varphi_{15} + \sin\delta_1\varphi_2$$
$$f_{13} \equiv \cos\eta_2\varphi_3 + \sin\eta_2\varphi_{13}$$
$$f_{14} \equiv -\cos\eta_2\varphi_{13} + \sin\eta_2\varphi_3$$
$$f_{15} \equiv \cos\eta_2\varphi_4 + \sin\eta_2\varphi_{14}$$
$$f_{16} \equiv -\cos\delta_2\varphi_{14} + \sin\delta_2\varphi_4.$$

C. As stated, the eigenkets for the energies, listed in order highest energy down to lowest energy, for all fields B, by definition are: $\varphi_1, \varphi_2, \ldots, \varphi_{15}, \varphi_{16}$.

References

[1] S.M. Nokhrin, J.A. Weil, D.F. Howarth, Magnetic resonance in systems with equivalent spin-1/2 nuclides. Part 1, J. Magn. Reson. 174 (2005) 209–218. Erratum: In various places, symbol "n" should not be italic. Thus for example in XL_n; italic "n" is to be reserved for situations when the meaning is to be "nuclear". There is a missing reference [PF87] on p. 210: C.P. Poole Jr., H.A. Farach, Theory of Magnetic Resonance, second ed., John Wiley & Sons, New York, NY, USA, 1987. On p. 211, line 9 on the right, −A/4 should be −3A/4. On p. 212 (lines 23-4), the sum formula should not have been split. Also on p. 212, various + and − signs appearing in groups of three within ket symbols should be equally spaced. Table 1 on p. 213: letter symbols A_1, A_2, E, T_1 and T_2 here should not be italic. On p. 215, line 2: letter symbol A_1 should not be italic. In various places, in denominators, symbols $g_e\beta_e$ should be placed within parentheses (). On p. 218, Ref. [28], there should be a comma after 'Lifshitz'..

[2] S.M. Nokhrin, D.F. Howarth, J.A. Weil, Magnetic resonance in systems with equivalent spin-1/2 nuclides. Part 2, J. Magn. Reson. 193 (2008) 1–9, doi:10.1016/j.jmr.2008.02.010.

[3] G. Baym, Lectures on Quantum Mechanics, W.A. Benjamin, New York, NY, USA, 1969.

[4] J.A. Weil, J.R. Bolton, Electron Paramagnetic Resonance—Elementary Theory and Practical Applications, second ed., John Wiley & Sons, New York, NY, USA, 2007.

[5] B. Bleaney, Part L. Hyperfine structure in paramagnetic salts and nuclear alignment, Phil. Mag. 43 (1951) 441–458.

[6] J.A. Weil, On the intensity of magnetic resonance absorption by anisotropic spin systems, in: J.A. Weil (Ed.), Electronic Magnetic Resonance of the Solid State, Canad. Soc. Chem., Ottawa, ON, Canada, 1987, pp. 1–19.

[7] J.A. Weil, M.J. Mombourquette, Computer Program EPR–NMR, Department of Chemistry, University of Saskatchewan, 110 Science Place, Saskatoon, SK, S7N 5C9, Canada 1995 (Version 6.5.3, 2007).

[8] R.W. Fessenden, R.H. Schuler, ESR spectra and structure of the fluorinated methyl radicals, J. Chem. Phys. 43 (8) (1965) 2704–2712.

[9] R.W. Fessenden, Second-order splittings in the ESR spectra of organic radicals, J. Chem. Phys. 37 (4) (1962) 747–750.

[10] W. Weltner Jr., Magnetic Atoms and Molecules, Van Nostrand Reinhold, New York, NY, USA, 1983.

[11] A. Abragam, B. Bleaney, Electron Paramagnetic Resonance of Transition Ions, Clarendon Press, Oxford, UK, 1970.

[12] G.E. Pake, T.L. Estle, The Physical Principles of Electron Paramagnetic Resonance, second ed., W.A. Benjamin, Reading, MA, USA, 1973.

[13] A. Carrington, A.D. McLachlan, Introduction to Magnetic Resonance, Harper & Row, New York, NY, USA, 1967.

[14] R.B. Griffiths, Consistent Quantum Theory, Cambridge University Press, Cambridge, UK, 2002.

[15] J.A. Weil, The life of π and σ — a tutorial review of the ubiquitous use of these symbols in Zeeman and magnetic resonance spectroscopy, Concepts Magn. Reson. A 32A (2) (2008) 134–142. Erratum: Unfortunately, the symbols π and σ appear reversed one time, on p. 140 just after the selection rules cited.